4.1 Introduction

Amorphous solid electrolytes possess some unique physical properties and hence to characterize and study their physical properties, various techniques and methods have been used. In the present chapter, the characterization results of prepared glass samples by their density and molar volume, powder X-ray diffraction, thermal properties by differential scanning calorimetry (DSC), structural characterization by Fourier transform Infra-Red spectroscopy (FTIR) are presented. Ionic transport number measurements by e.m.f. method to find out the percentage contribution of mobile cations towards total conductivity of the prepared glass samples. Electrical and transport properties have been discussed in chapter 4 in detail.

4.2 Density and molar volume

Density of the prepared samples was measured by Archimedean principle using methanol as the immersion fluid. The density of the prepared glass samples is calculated using the following formula,

$$\rho_{sample} = \rho_{liquid} \times \left(\frac{M_{air}}{M_{air} - M_{liquid}} \right) \qquad \ldots\ldots\ldots (4.1)$$

where,

ρ_{sample} = density of the sample
ρ_{liquid} = density of the immersion liquid
M_{air} = mass of the sample in air
M_{liquid} = mass of the sample in liquid

The obtained density values as function of composition are shown in Fig. 4.1, and it increases monotonically with increasing concentration of PbI_2, suggesting a consistent reduction in inter ionic distances.

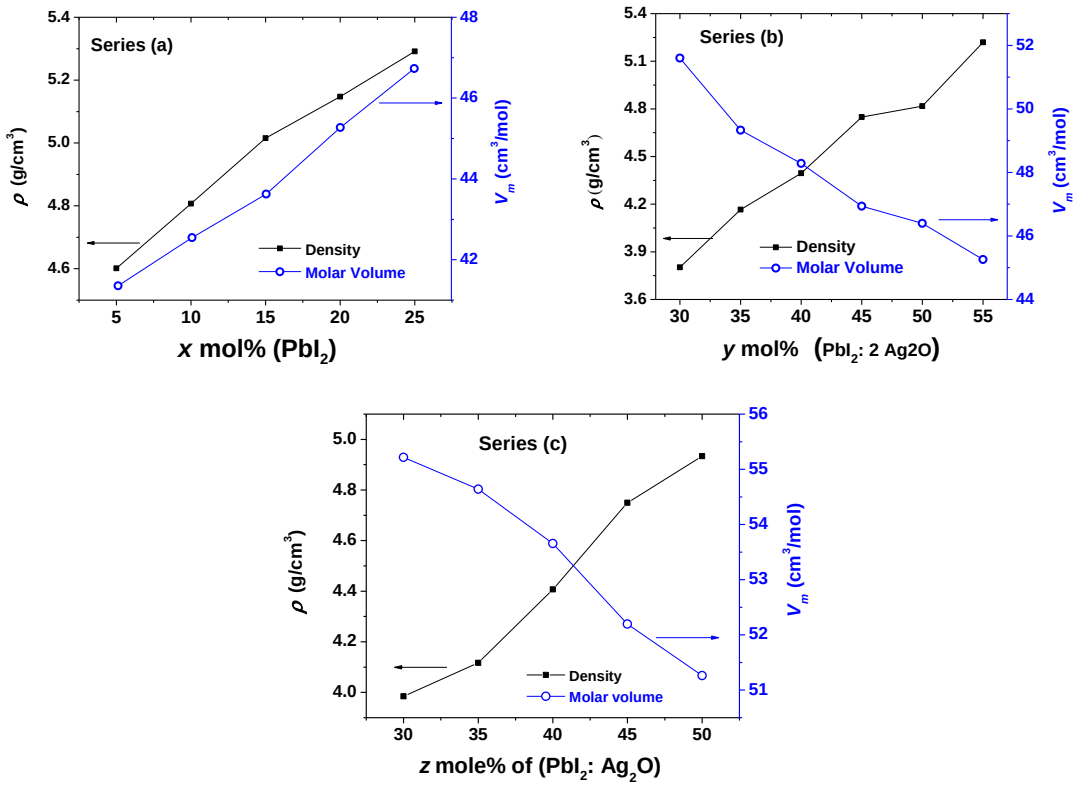

Fig. 4.1. Density, ρ, and molar volume, V_m of glass samples for all series.

In general, density of glasses is explained in terms of a competition between the masses and sizes of various structural units present therein. In other words, density of a glass is related to how tightly the ions and ionic groups are packed together in the structure [1].

The molar volume, V_m, of the prepared glass samples was calculated using the following equation [2],

$$V_m = \frac{M}{\rho} \qquad \ldots\ldots\ldots (4.2)$$

where, M is the molar mass of the glass sample, and is given as $M = \Sigma\, C_i A_i$, C_i and A_i are molar concentrations and molecular weight of the i^{th} component respectively and ρ is the measured density of the corresponding sample.

Drake *et al.* [3] proposed that the monotonic change of molar volume with composition suggests that the network structure of glass does not change. Fig. 4.1

signifies that the molar volume decreases monotonically and structure of the glass network should be shrinking with increasing PbI_2 content. Table 4.1 shows a summary of density, molar volume, distance between Vanadium-Vanadium ions and Ag-Ag ions.

Table 4.1 Density, Molar Volume, Vanadium-vanadium and Silver-Silver Spacing for all glass compositions

Glass Series	mole%	ρ (g/cm^3)	V_m (cm^3)	V-V spacing (Å)	Ag-Ag spacing (Å)
Series (a)	5	4.601	41.356	4.262	4.768
	10	4.807	42.549	4.381	4.901
x PbI_2 - (100-x)	15	5.015	43.624	4.503	5.037
[Ag_2O - 2(0.7V_2O_5	20	5.148	45.272	4.652	5.204
– 0.3B_2O_3)]	25	5.292	46.732	4.804	5.374
Series (b)	30	3.802	51.598	4.438	5.983
	35	4.166	49.017	4.472	5.587
y (PbI_2:2Ag_2O) -	40	4.395	48.282	4.570	5.317
(100-y) [0.7V_2O_5 -	45	4.748	47.362	4.641	5.044
0.3B_2O_3]	50	4.818	46.373	4.825	4.904
	55	5.219	45.255	4.922	4.679
Series (c)	30	3.984	55.216	4.243	6.736
	35	4.117	55.441	4.374	6.407
z (PbI_2:Ag_2O) -	40	4.407	53.656	4.466	6.062
(90-z) V_2O_5 -	45	4.750	51.514	4.563	5.750
10B_2O_3	50	4.933	51.262	4.738	5.542

4.3 X-ray Diffraction studies.

X-ray diffraction pattern for all five glass compositions of series (a) is shown in Fig. 4.2 below. It is observed that in this glass series, all compositions, except x = 25 mole% PbI_2 doped, exhibit a broad halo like curve characteristic of amorphous substance, in low 2θ region (25˚ to 35˚), which confirms that these compositions must be fully amorphous in nature. The x = 25 mole% composition appears with a broad halo in the same 2θ region as observed for other compositions, except three sharp peaks appearing at 2θ = 23.69˚, 39.26˚ and 46.41˚ values. A comparison with

the ICDD-JCPDS files [4, 5] confirms the crystalline aggregate belonging to AgI; i.e. stabilization of AgI in the amorphous host glass network must have taken place.

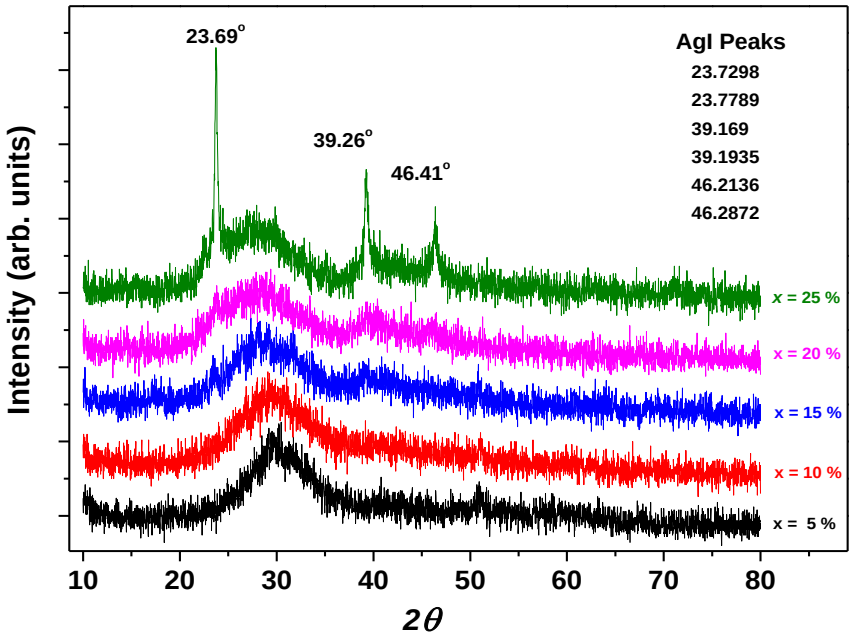

Fig. 4.2. X-ray diffraction patterns for all compositions of glass series (a).

As can be noted that this particular glass composition is having equal amounts of PbI_2 and Ag_2O concentrations, hence it is likely that all PbI_2 and Ag_2O molecules might have undergone the exchange reaction process, and therefore a large amount of AgI should have been created which might have remained un-dissolved partially in the host glass network and making AgI clusters. This confirms the solubility limit of PbI2 in this glass system. This finding is also supported in the DSC scan of x = 25 mol PbI_2 by a sharp endothermic peak near 149 ˚C which is very close to the $\beta \rightarrow \alpha$ transition of AgI.

X-ray diffraction pattern for all glass compositions of glass series (b) & (c) is shown in Fig. 4.3 & 4.4 respectively. As observed from these figures no sharp peaks are observed, instead only a broad peak between 2θ = 25˚ to 30˚ region, which is a

fingerprint of fully amorphous materials. And it confirms the amorphous nature of the compositions of glass series (b).

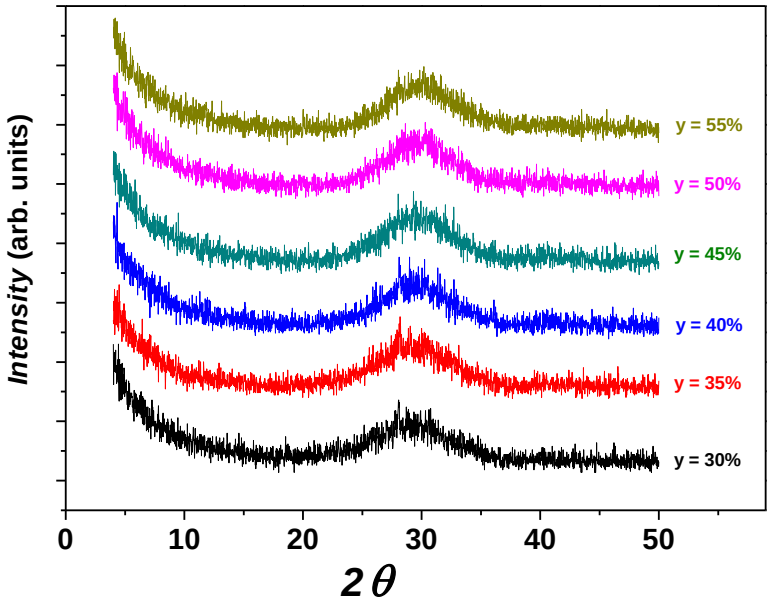

Fig. 4.2. X-ray diffraction patterns for all compositions of glass series (b).

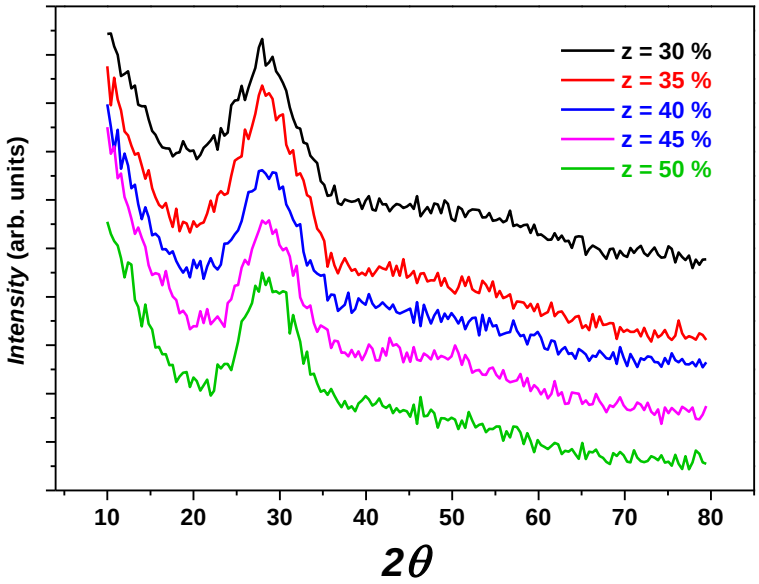

Fig. 4.4. X-ray diffraction patterns for all compositions of glass series (c).

The peak free XRD patterns suggest that no crystallization has occurred, and the prepared samples are purely amorphous and glassy in nature. Further

confirmation of crystallinity of these prepared glass samples has been made by analyzing their DSC scans.

4.4 Differential Scanning Calorimetry Studies

In addition to, being x-ray amorphous, a glass must exhibit glass transition behavior as well. "Glass transition is defined [6] *as that phenomenon in which a solid amorphous phase exhibits with changing temperature a more or less sudden change in the derivative thermodynamic properties such as heat capacity and expansion coefficient, from crystal-like to liquid-like values"*. The temperature of transition is known as glass transition and is denoted as T_g.

In order to detect the glass transition behavior, glass transition temperature and subsequent crystallization of the amorphous phase, a Differential Scanning Calorimetry (DSC) is the most suitable technique.

In a DSC experiment, the difference in the amount of heat energy (enthalpy) required to keep both the test sample and the reference are heated at a constant heating rate simultaneously at a constant heating rate. A plot of energy (enthalpy) versus temperature is obtained and it is called a DSC scan. In a DSC plot, the x-axis represents temperature and y-axis represents the difference of heat flow between the test sample and the reference. A number of peaks relating to endothermic or exothermic nature are observed which may be used as a means for the qualitative identification of the substance under investigation. In most commercially available DSC instruments, heating rates of 1 to 100˚C per minute are available. When heating is started, the heat is either absorbed or released by the material against temperature If the horizontal line in the DSC scan shifts downwards (endothermic direction), it means that heat is being absorbed by the sample and a change in its

heat capacity has occurred. This particular temperature is known as 'glass transition temperature' T_g. At melting transition, the molecular/polymeric chains come out of their ordered arrangements and begin to move around freely. When the substance crystals melt, they must absorb heat. Such endothermic peak is known as melting temperature. In between these two endothermic peaks, an exothermic peak is also observed called crystallization peak. Above the glass transition, the molecules have a lot of mobility and they may rearrange to form very ordered arrangements, called crystals. When the substance fall into these crystalline arrangements, they give off heat and it can be seen as an exothermic peak in the plot of heat flow versus temperature plot in a typical DSC experiment. The temperature at this highest point is usually considered to be the substance crystallization temperature denoted as T_c.

In case of amorphous solid electrolytes or Fast Ion Conducting (FIC) glasses, the knowledge of T_g and T_c as well as melting temperature T_m are essential. Because, the conductivity and other transport properties of FIC glasses are highly temperature dependent (usually increase with increasing temperature) and tend to show abrupt behavior at various transition temperatures such as T_g, T_c or T_m where a lot of molecular motions are involved, which affects their conductivity greatly. Moreover, FIC glasses are considered to be decoupled material systems, where motions of mobile ions are decoupled from the rigid glass network. In order to know the decoupling index of the glass materials, knowledge of the glass transition temperature is a must.

Hence, in order to study the thermal behavior of the glass systems, their DSC scans were recorded at a heating rate of 10˚C/minute from room temperature to just before their melting temperature. DSC scans recorded for the glass series (a), (b) and (c) are presented in Fig. 4.5, 4.6 and 4.7 respectively. The general observation of

these DSC scans is that they reveal an endothermic baseline shift corresponding to the glass transition, followed at higher temperatures by an exothermic peak occurring due to crystallization of the amorphous phase. For most samples, two distinct and well separated crystallization peaks are observable, which means that either two different crystallization phases are occurring these temperatures or the first crystalline phase itself might be undergoing re-crystallization, and hence an excess heat evolves as T_{c2} exothermic peak. The glass transition temperature and crystallization temperature have been summarized in tables 4.2, 4.3 and 4.4 below the respective DSC plots for each glass series.

Fig. 4.5 shows the DSC scans for all compositions of the glass series (a): $x$$PbI_2$-(1-$x$)[$Ag_2O$-2(0.7$V_2O_5-0.3B_2O_3$)], with varying PbI_2 concentration. It is observed that all samples show the presence of an endothermic baseline shift between 75 to 100˚C and is followed by two well separated crystallization peaks. The glass transition temperature and crystallization temperatures Tc_1 and Tc_2 are given in Table 4.2. The x = 25 mole% PbI_2 containing sample shows two endothermic transitions one at 82˚C and another at 149˚C. The first endothermic transition is assigned to the glass transition of this sample. While, the second endothermic transition occurring at 149˚C is very sharp implying melting transition. Occurrence of such melting transition near 149˚C has been reported by Berbenni *et al.* [7] and Tatsumisago *et al.* [8] for AgI-Ag_2O-B_2O_3 glasses containing large amounts of AgI. This endothermic peak has been assigned to the $\beta \rightarrow \alpha$ phase transition of aggregates of AgI in glass. Such aggregates in x = 25 mole% composition are possible because of the large amount of formation of AgI which occurs due to the exchange reaction between PbI_2 and Ag_2O which might not have dissolve completely in this particular sample.

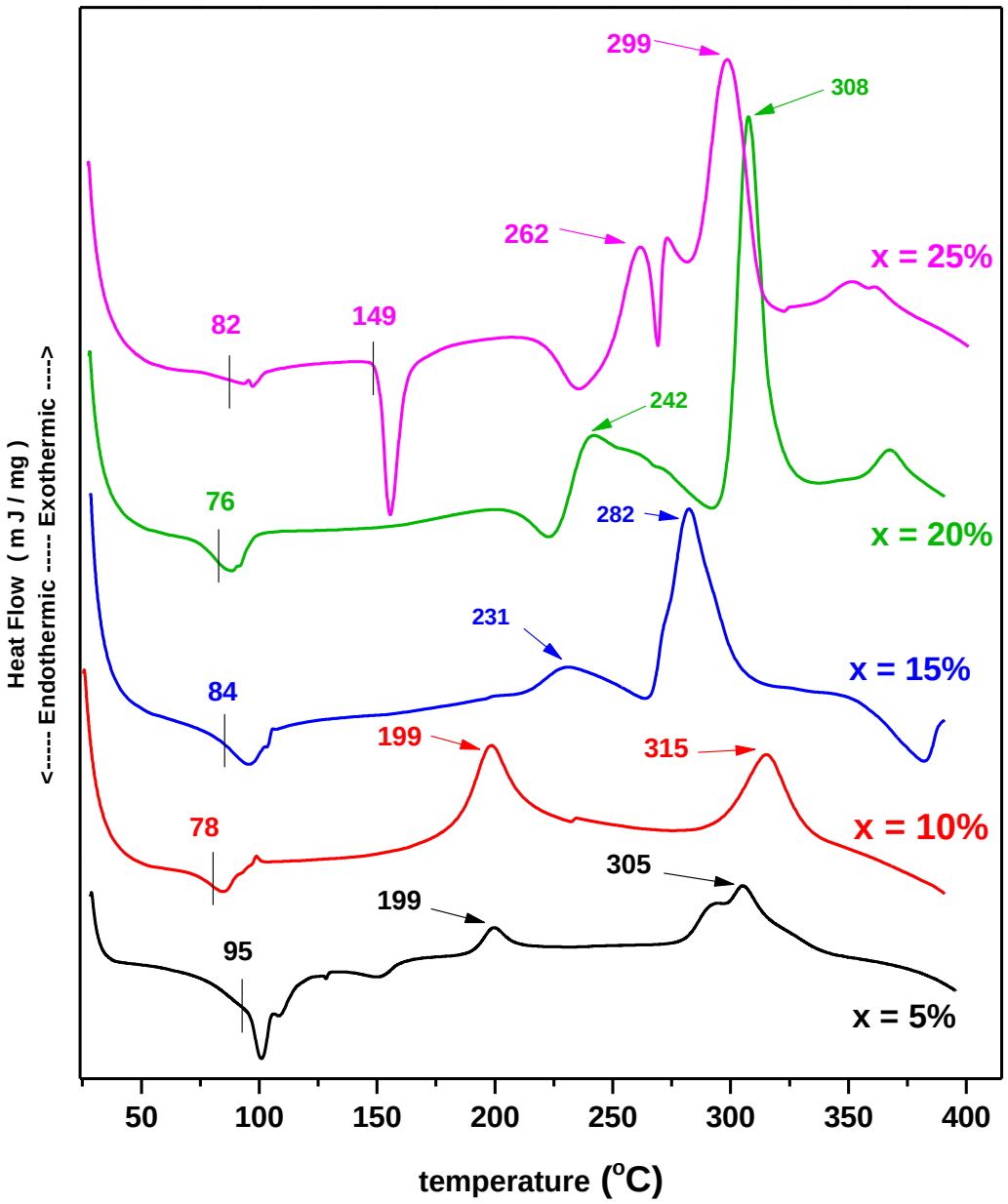

Fig. 4.5. DSC thermograms of all samples of glass series (a)

(*Y axis is in arbitrary units*).

Table 4.2: Glass transition temperature and crystallization temperature for glass series (a) obtained from DSC scans.

x mole%	T_g (˚C)	$Tc_1 - T_g$ (˚C)	Tc_1 / T_g	Tc_1 (˚C)	Tc_2 (˚C)
5	95	105	2.09	199	305
10	78	121	2.55	199	315
15	84	147	2.75	231	282
20	76	166	3.18	242	308
25	82	180	3.20	262	299

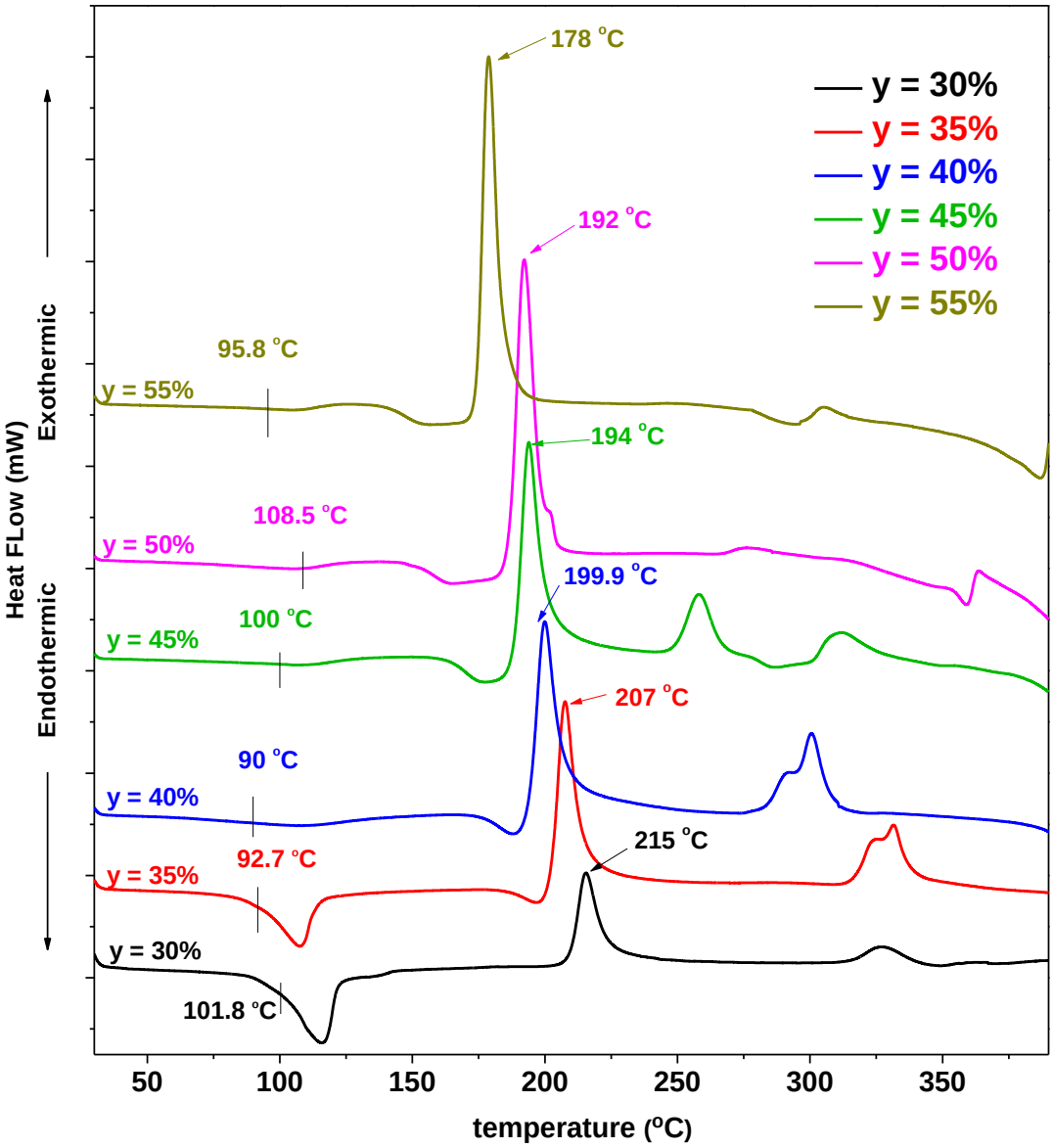

Fig. 4.6. DSC thermograms of all samples of glass series (b)
(*Y axis in arbitrary units*)

Table 4.3: Glass transition temperature and crystallization temperature for glass series (b) obtained from DSC scans.

y mole%	T_g (°C)	$Tc_1 - T_g$ (°C)	Tc_1 / T_g	Tc_1 (°C)	Tc_2 (°C)
30	102	113	2.11	215	327
35	93	114	2.23	207	326
40	90	109.9	2.22	199.9	300
45	100	94	1.94	194	258
50	109	83	1.76	192	200
55	96	82	1.85	178	—

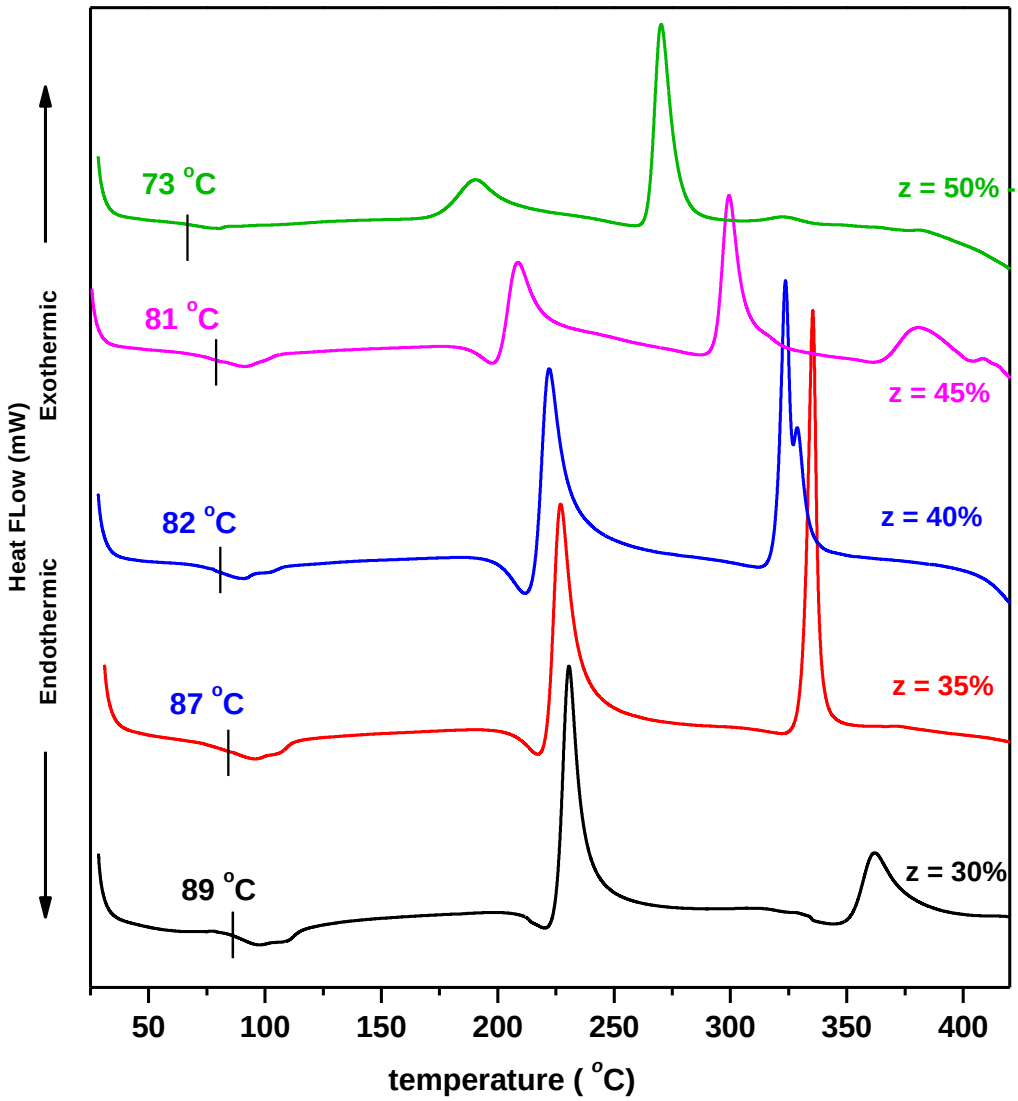

Fig. 4.7. DSC thermograms of all samples of glass series (c)
(*Y axis in arbitrary units*)

Table 4.4: Glass transition temperature and crystallization temperature for glass series (c) obtained from DSC scans.

z mole%	T_g (˚C)	$Tc_1 - T_g$ (˚C)	Tc_1 / T_g	Tc_1 (˚C)	Tc_2 (˚C)
30	89	142	2.596	231	362
35	87	140	2.609	227	335
40	82	140	2.707	222	324
45	81	128	2.580	209	299
50	73	117	2.603	190	270

Presence of aggregates of AgI has been evidenced by x-ray diffraction scans of this particular composition as depicted in Fig. 4.2, where three characteristics peaks of AgI appear in the amorphous background and are found to be belonging to α-AgI phase. And that is why, when the x = 25 mole% PbI_2 containing glass sample is heated, the AgI aggregates undergo a $\beta \rightarrow \alpha$ phase transition, and a sharp endothermic peak near 149˚C evolves.

DSC scans of the glass compositions of the series (b): y (PbI_2:$2Ag_2O$) - (100-y) [$0.7V_2O_5$ - $0.3B_2O_3$] ; are shown in the Fig. 4.6. It is observed that, for each of the glass compositions, a well defined glass transition is observed between 90 to 110˚ C and is followed by an exothermic peak of crystallization. Except for y = 50 & 55 mol% compositions, other samples show two distinct crystallization peaks. It is observed that the temperature difference between these two crystallization peaks reduces gradually with increase in x mol% of (PbI_2:$2Ag_2O$). The T_g, Tc_1 & Tc_2 values are given in Table 4.2. It is noted that the glass transition values decrease initially with increasing y mole% of (PbI_2:$2Ag_2O$) and become minimum at 40 mole% and then again start increasing upto 50 mole% and suddenly drop at 55 mole%. The observed minimum in T_g values suggests that the glass structure must be getting softened due to increasing amount of the modifier content Ag_2O as well as lead ions in the vanado-borate network till 40 mole%, however after this particular composition onwards, the increase in T_g may be devoted to the increased concentration of PbO as well as V=O bonds as seen in their respective FTIR spectra. However it is interesting to note that both Tc_1 & Tc_2 decrease systematically with increasing PbI_2 & Ag_2O content. The non-systematic decrease in T_g might be occurring due to the reason that all these glasses were quenched manually and hence

even a little difference in the quenching rate of the glass melt might have resulted in such reduction in temperature. The fall in Tc_1 and Tc_2 is ascribed due to the formation of PbO due to the exchange reaction on the glass system, which is playing a role of modifier. Occurrence of two different peaks of crystallization suggests the formation of two different crystalline phases which crystallize at different temperatures.

For the third glass series (c): z (PbI_2:Ag_2O) - (90-z) V_2O_5 - $10B_2O_3$; where only the glass former V_2O_5 is being varied, the DSC scans are shown in Fig. 4.7. Following observations are made from these scans.

(1). The glass transition is followed by two well defined exothermic crystallization peaks, which are well separated from each other.

(2). T_g is reducing systematically with decreasing V_2O_5 content.

(3). The first crystallization shifts towards lower temperature with the decreasing V_2O_5 content.

(4). The difference between Tc_1 and Tc_2 also reduces with decreasing V_2O_5 content.

In this system, the V_2O_5 decreases at the expense of the glass modifier and the dopant PbI_2. Empirical observation by Rawson [9] in a mixed glass former network showed that increasing V_2O_5 brings a decrease in glass transition temperature. Because of the formation of higher number of ionic bonds that occur due to increasing concentration of mobile Ag^+ ions. Garbarczyk *et al.* also showed similar behavior in Li_2O-V_2O_5-P_2O_5 glass system [10].

4.5 Fourier Transform Infrared Spectroscopy analysis

Fourier transform infrared (FTIR) spectroscopy is a powerful tool to investigate the structural details of materials. The chemical interactions may result in band shifts and broadening. Infrared spectroscopy measures the vibrational energy levels in the region of different molecules. FTIR spectra of materials vary according to their compositions and show the interaction between the various constituents.

In glasses, the vibrational bands are generally broader and overlapping than those observed in crystalline materials. This is because of the lack of long range order in glasses and is similar to the broadening of the spectra observed in other techniques [11-14] .The infrared transmittance spectra of the presently investigated glasses have been recorded in order to obtain information about the possible changes in vibrational spectra. Different glass compositions due to variation in doping concentration as well as in modifier and former concentrations may result structural grouping rearrangements of vibrational spectra which can be studied with FTIR spectroscopy.

In the present glass systems (a, b and c series), PbO, V_2O_5 and B_2O_3 are the glass formers /conditional glass formers. Presence of BO_3, V-O-V, PbO and V=O etc. structural units have been observed in these glasses from the study of FTIR spectra. V_2O_5 and B_2O_3 structures are consisted of deformed VO_5 trigonal bonded in zigzag chains and randomly oriented three dimensional networks of BO_3 triangles, respectively. B_2O_3 is a network former with BO_3 and BO_4 structural units. When PbI_2 and Ag_2O are incorporated into B_2O_3 matrix, they convert BO_3 structural clusters into more stable BO_4 units and may also form non-bridging oxygen. FTIR spectra of all samples (Fig. 4.8 to 4.10) show the broadened absorption bands which

are the characteristic of the random structure with a wide distribution and indicate lack of long range order [16].

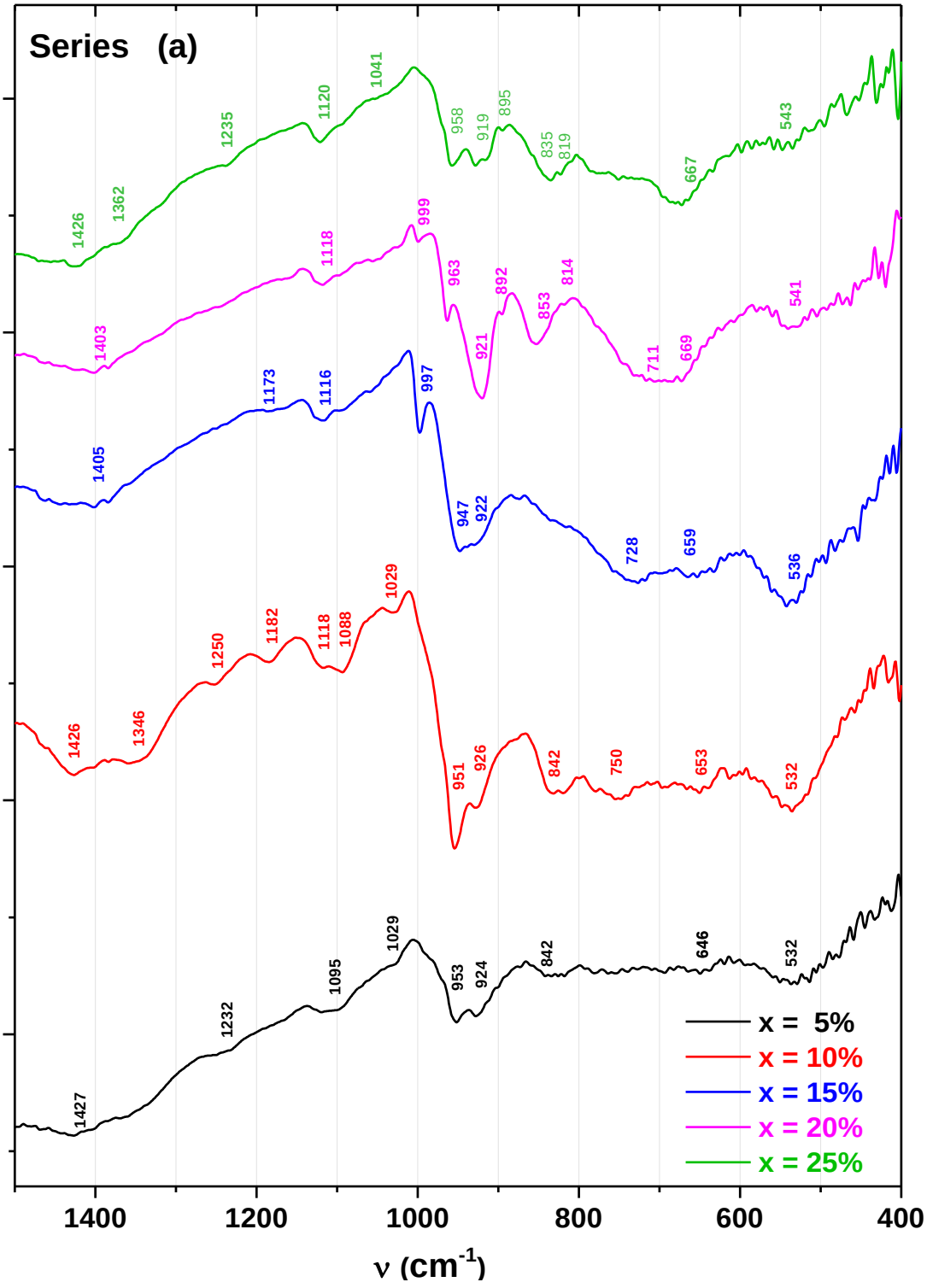

Fig. 4.8. FTIR spectra of glass series (a): *x* PbI_2 - (100-*x*) [Ag_2O - 2($0.7V_2O_5$ – $0.3B_2O_3$)].

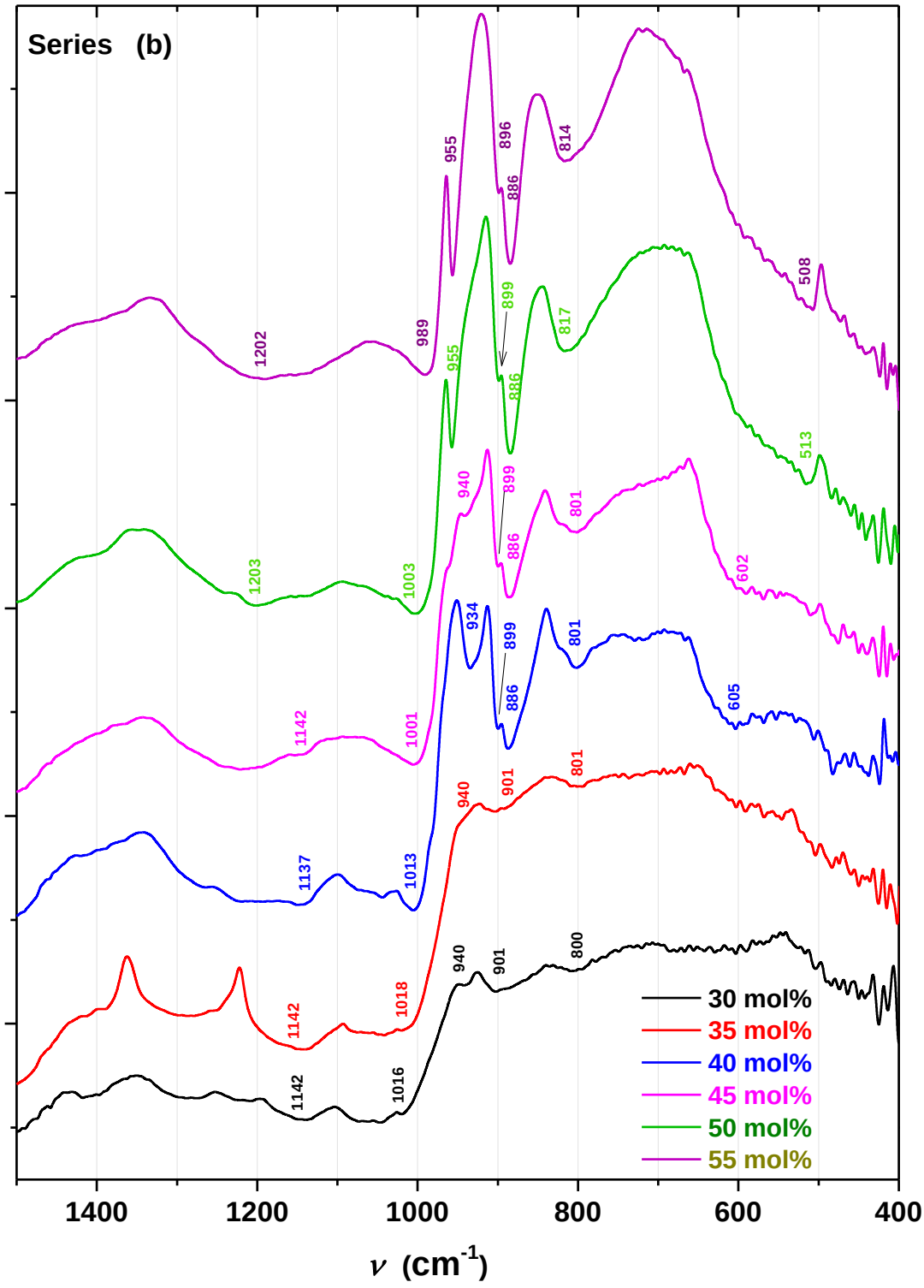

Fig. 4.9. FTIR spectra of glass series (b): y (PbI_2:2Ag_2O) - (100-y) [0.7V_2O_5 - 0.3B_2O_3].

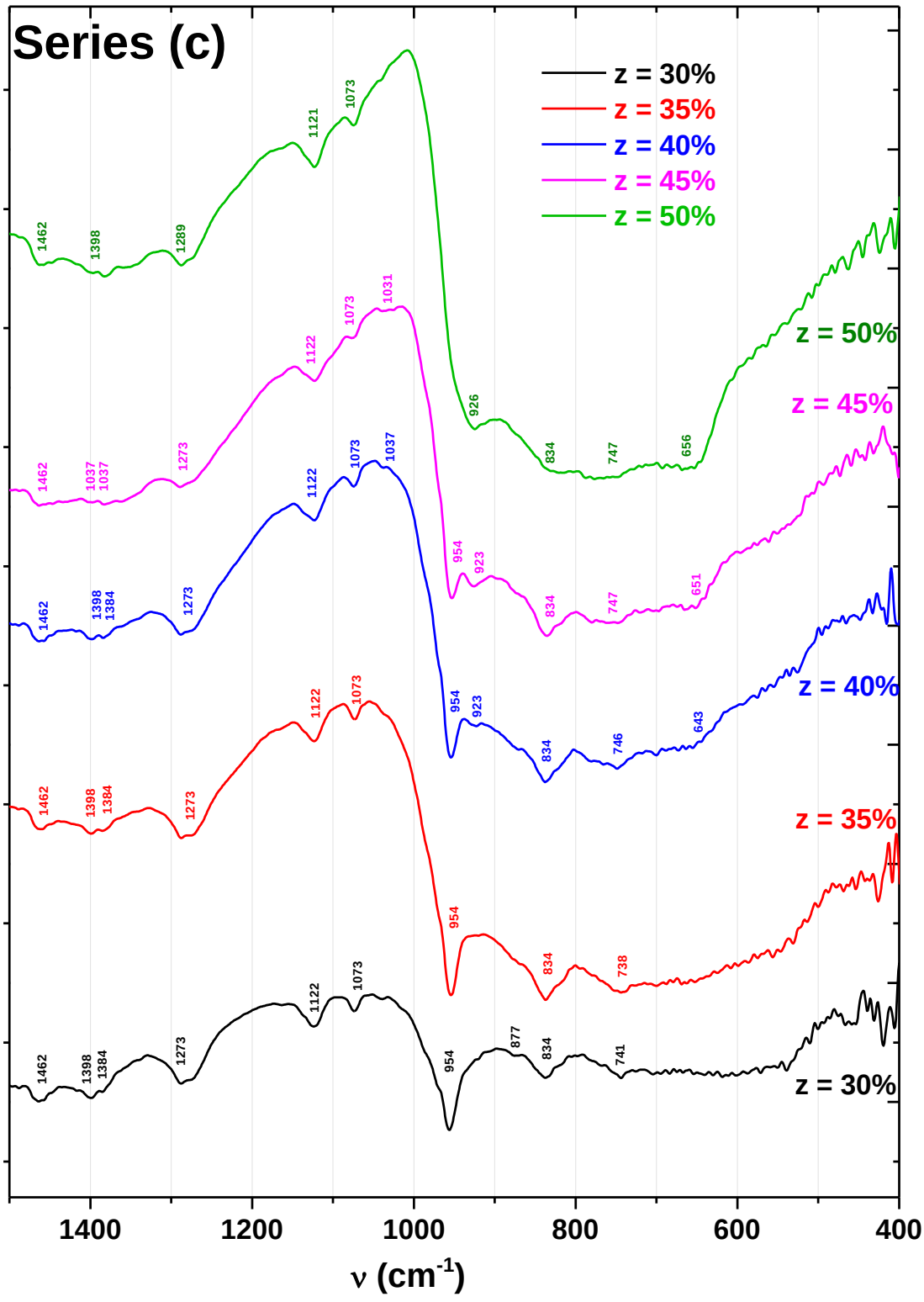

Fig. 4.10. FTIR spectra of glass series (c): *z* (PbI_2:Ag_2O) - (90-*z*) V_2O_5 - 10B_2O_3 .

This also depends upon whether PbO, from exchange reaction between PbI_2 and Ag_2O, will go into modifying positions or network forming positions. Satyanaryana [15] suggested that PbO participates in the glass network both with covalent and ionic bonding and participate in the glass network with [$PbO_{4/2}$] pyramidal units. Fig. 4.8 depicts the room temperature FTIR spectra obtained for various compositions of lead iodide containing silver borovanadate **glass series (a).** In this series the PbI_2 concentration is varied in order to see the effect of doping of lead iodide in the structure of silver vanado-borate glass matrix. In this system, the dopant salt PbI_2 concentration is varied from 5 to 25 mole% with respect to remaining glass composition. In figure, the significant peaks are observed at 1435-1424, 1385-1340, 1253, 1119, 952, 836, 818, 751, 649, 533 and 463-419 cm^{-1} frequencies.

The vibrational bands present in the region of 1430-1410 cm^{-1} and 838-818 cm^{-1} are due to the B-O stretching vibrations of BO_3 units in chain and ring type metaborate and BO_4 groups. While the absorption peak near 1330 cm^{-1} region is assigned to the B-O stretching vibration of BO_3 units in pyroborate groups. The IR band around 1220 is accredited to B-O stretching vibrations of $(BO_3)^{3-}$. The vibration band at 1090 cm^{-1} is assigned to the PbO asymmetrical bending vibration. The high frequency band appearing near 950 cm^{-1} (957-948 cm^{-1}) is attributed to VO_5 structural units as well as to the branched VO_4 units having VO_4 bond. The bands in the region 836-818 cm^{-1} are ascribed to vibrations of V-O-V chains as well as BO_3 units and BO_4 groups. The absorption bands located in the region of at 670-645 cm^{-1} are due to Pb-O bonds vibrations of PbO_n units with n=2 and n=4 [17]. The bands at 530-500 cm^{-1} are attributed to the vibrations of angular deformation of the V-O bonds.

From Fig. 4.8, it is clear that as the doping concentration (PbI_2 content) increases, the absorption bands located at 952 and 929 cm^{-1} become more intense, however, at x =15% these bands produce a wide broad band. This shifting of bands towards higher wavenumber side indicates the existence of the $VO_5 \rightarrow VO_4$ conversion process. The band observed in the region of 1100-1060 cm^{-1} is attributed to the presence of BO_4 groups. The characteristic vibrations of the isolated vanadium-oxygen bonds in the IR spectrum are in the range of 1020-900 cm^{-1} [18]. The band at 1020 cm^{-1} is related to the vibrations of the non-bridging V=O of the VO_5 groups [19]. The intensity of this band decreases with decreasing V_2O_5 content along with a change in position towards lower wavenumber. The absorption bands occur at 850 cm^{-1} frequency for x =10, 20 and 25 mol % samples. This band is attributed to the asymmetric vibrations along the V-O-V bonds involved in the corner sharing of VO_5 polyhedra [19].The vibrational bands in the 530-541 cm^{-1} is assigned to PbO symmetrical bending vibrations. All samples show a strong and easily distinguishable absorption bands from 1000-900 cm^{-1}.

FTIR spectra of second **glass series (b)** in which the ratio of PbI_2 and Ag_2O has been kept constant and its concentration is varied with former content from 30 to 55 mole % series [$y(PbI_2{:}2Ag_2O)$-$(1-y)(0.7V_2O_5$-$0.3B_2O_3)$], is depicted in Fig. 4.9. The various significant absorption peaks that are being observed here are at frequencies 1435-1424, 1385-1340, 1328, 1220, 1090, 975, 950, 851-832, 820, 665-628, 530-500 and 467-440 cm^{-1} in different compositions. The IR absorption bands in 1585-1340 cm^{-1} region are assigned to the B-O stretching vibrations of BO_3 units in pyroborate groups with the standard frequency being ~1328 cm^{-1}, which is found to be present in all of the samples. Now in y = 30 mol% ($PbI_2{:}2Ag_2O$) composition,

peaks appearing at 1018, 937, 905, 811 and 795 cm^{-1} are assigned to V=O, PbO, VO_4, B-O-B linkages and VO_4 tetrahedra respectively. It is observed that for the composition, y = 35 mol% the same peaks appear as in the case of y = 30 mol% and at same position i.e. glass structure does not seem to change. It is observed that at 40 mol% some new peaks appear or get stronger or shift significantly. These peaks are present at 1004, 935, 898, 822 and 801 cm^{-1} position. It may be noted that the peak 1018 cm^{-1} that is due to V=O oscillations in y = 30 mol%, keeps on shifting gradually towards lower frequency side with increasing PbI_2:$2Ag_2O$ concentration/ reducing V_2O_5+B_2O_3 concentration suggesting a gradual elongation of the V=O bond in VO_5 tetrahedral units [20]. The peak at 937 cm^{-1} which is due to Pb-O symmetrical stretching vibrations in y = 30 and 35 mol% seems to be shifted towards higher frequency side at 941 and 957 cm^{-1} for y = 45 and 50 mol% compositions respectively. It is suggested that with increasing concentration of PbI_2:$2Ag_2O$ in the glass network, the Pb-O bond is getting stronger. In addition to this, the band appearing at 510 cm^{-1} in y = 30 mol% which is devoted to the Pb-O symmetric bending vibrations, is found to shifting towards higher frequency side gradually with increasing y mol% and its intensity also grows. The shifting in V=O towards lower side and of Pb-O towards higher frequency side suggests that PbO is interacting with the increasing PbO content, the interaction between PbO and the double bond of V=O from VO_5 is increasing [21-23] . Ganguli *et al.* [24] have reported that this is possible when PbO is playing the role of a network former. This is reflected when we consider the molar volume, which is found to increase with increasing concentration of V_2O_5. The composition at which PbO changes its role from that of a modifier to network former may be understood as follows:

"PbO may enter into the glass network only as $[PbO_{4/2}]^{2-}$ unit where it competes with B_2O_3 for the oxygen available from the modifier Ag_2O, since PbO is identically $[PbO_{2/2}]^0$, and following reaction should take place,

$$[PbO_{2/2}]^0 + O^{2-} \rightarrow [PbO_{4/2}]^{2-}$$

Thus the addition of PbO can be considered as taking away O^{2-} ions from the modified vanadoborate network. And it is noted that PbO and V=O bonds are interacting.

In the FTIR spectra of the **third glass series (c)**, where the ratio of PbI_2: Ag_2O is kept constant 1:1 and the amount of glass former V_2O_5 is reducing against it, is shown in Fig. 4.10. It is observed that the peaks appearing at 1462, 1398, 1384, 1288, 1273, 1122, 1072 and 1038 cm^{-1} remain almost unchanged in all of the compositions in terms of peak height as well as peak positions. The peaks at 1462,1398,1384,1286 and 1273 cm^{-1} are assigned to the BO_3 units while the peaks at 1122 and 1074 cm^{-1} are indicative of the presence of NBOs in BO_4 structural units. It may be noted that amount of B_2O_3 has fixed at 10 mol% in all the compositions in this particular series and hence it might be reason, therefore that the peaks for borate structural units do not show any shifting peak positions from composition to composition. Also the peak at 744 cm^{-1} that is due to B-O-B stretching vibrations has also remained unchanged. The V=O bond is found to be shifted a little towards higher frequency side at 1038 cm^{-1} and is visible only as a very peak, even though these samples are containing very large amount of V_2O_5.

The peak appearing at 956 cm^{-1} is devoted to the symmetrical stretching vibrations of Pb-O from different structural units This peak keeps on decreasing intensity from x = 30 to 45 mol% and remains unchanged in position. A new peak at

923 cm^{-1} appears in z = 40 mol% glass composition is assigned to the Pb-O-Ag specific vibrations and its intensity keeps on increasing with increasing PbI_2:Ag_2O concentration. It is observed that the peaks at 925 and 957 cm^{-1} merge in z = 50 mol% PbI_2:Ag_2O (40% of V_2O_5) containing sample. Moreover, it may be noticed that this peak at 923 cm^{-1} is growing at the expense of the peak at 957 cm^{-1} which is devoted to the Pb-O bond vibrations. Hence it may be concluded that a growing interaction between PbO and Ag^+ might be responsible for such behavior. The absorption peak at ~ 837 cm^{-1} is devoted to V-O-V symmetric bending vibrations and its position remains unaltered. However, its intensity reduces gradually with decreasing V_2O_5 content.

A summary of the different functional groups present in the present glass systems is summarized in tables 4.5, 4.6 and 4.7 for glass series (a), (b) and (c) respectively.

Table 4.5: Summary of FTIR Absorption features & their Assignments for glass Series (a): *x* PbI_2 - (100-*x*) [Ag_2O - 2(0.7V_2O_5 – 0.3B_2O_3)].

Wave number (cm^{-1})	Behavior	Assignment
1118	No change	NBOs in B-O units
1095	No change	BO_4 groups [25]
103	Shifting to lower side	
953	Unaltered position	• VO_5 a as well as V=O bond in VO_4 units • Pb-O symmetrical stretching vibrations
924	Unaltered	Pb-O-Ag linkages
871	Shift to higher side	
842	Shift to lower side	V-O-V symmetrical/asymmetrical bending
646	Shift to higher side upto 675 cm-1	B-O-B bending of trigonal BO_3 units
463	No change	PbO_4 units

Table 4.6: Summary of FTIR Absorption features & their Assignments for glass Series (b): y (PbI_2:$2Ag_2O$) - (100-y) [$0.7V_2O_5$ - $0.3B_2O_3$].

Wave number (cm^{-1})	Behavior	Assignment
1140	Disappears after 45 mole%	BO_4 stretching vibrations
1018	Shift to lower side	• BO_4 tetrahedra • Due to higher content of V_2O_5
937	Shift to higher side	• V=O bond → the glass is getting stronger • Pb-O symmetric stretching vibrations
905	Shift to lower side	• Stretching of tetrahedral boron • Stretching of four connected five coordinated vanadium ion in VO_4
886	Unaltered position with increasing PbI_2 content	Nonbridging V-O bonds in VO_4 polyhedra. Stretching vibrations
811	Very weak and shifting to higher side. Absent in y = 50 and 55 mole% samples	B-O-B linkages
795	Shift to higher frequency side gradually	• V-O-B linkages • VO_4 tetrahedra without bridging

Table 4.7: Summary of FTIR Absorption features & their Assignments for glass Series (c): z (PbI_2:Ag_2O) - (90-z) V_2O_5 - $10B_2O_3$

Wave number (cm^{-1})	Behavior	Assignment
1462, 1398, 1384, 1273	Position unaltered	BO_3 units : these peaks appear at higher frequencies than for pure B_2O_3
1122	Constant position with no change in intensity	NBOs in B-O units
1072	Intensity decreases with increasing z mole%	BO_4^{-5} units [26]
1038	Very weak shoulder type peak	V=O bond's vibration in V_2O_5
956	Almost unaltered in position as well as height	• Pb-O • VO_5 and V=O bond in VO_4 units
918	intensity increasing upto 40 mole% an than decreasing 40 mole% onwards	Pb-O-Ag linkages due to interaction between mobile Ag^+ ions and $[PbO_{4/2}]^{-2}$ units.
837	No change	V-O-V linkages shifted to higher frequency side
744	Gradually shifting towards high frequency side	B-O-B vibrations of BO_3 and BO_4 groups
640	Appears at 45 and 50 mole% only	Due to bending vibrations of B-O-B bond

4.6 Ionic transport number

To confirm the super ionic nature of the prepared samples, the ion transport number of ionic species in the glass samples was determined using the e.m.f. technique [27, 28]. For this purpose, as mentioned in section 2.3.6, electrochemical cells were fabricated and immediately after that the Open Circuit Voltage (OCV) was measured. The transport number can be calculated by using the equation 4.3

Ionic transport number was measured using the e.m.f. of the electrochemical cell method. For this purpose, a standard cell for each glass composition was made in the following combination and measured its open circuit voltage to confirm its transport number using the formula given in equation 4.3. In the present case we have Ag^+ ion conductor, so the following composition of the cell was fabricated:

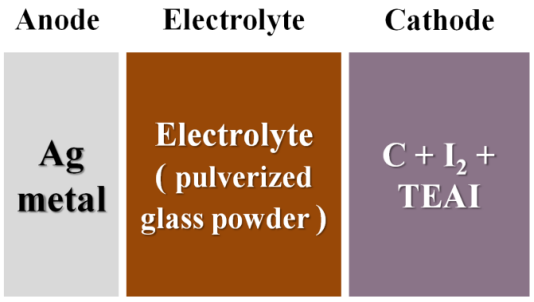

Ag (*metal*)	**Electrolyte** (*glass sample*)	***C + I_2 + TBAI*** (*cathode*)

where, Ag (metal) acts as anode and cathode consisted of ***C + I_2 + TBAI.*** (TBAI = *Tetra Ethyl Ammonium Iodide*). The following cell reaction occurs at anode and cathode of the cell,

At anode : $Ag \rightarrow Ag^{+} + e^{-}$

At cathode : $I_2 + 2\,e^{-}\ (\text{from external circuit}) \rightarrow 2\,I^{-}$

&

$2\,Ag^{+}\ (\text{through electrolyte}) + 2\,I^{-} \rightarrow 2AgI$

The standard e.m.f. for the above cell reaction is 0.687 V. Hence the ionic transport number t_{ion} can be calculated using the equation:

$$t_{ion} = \frac{Cell_{e.m.f.}}{0.687} \times 100\% \qquad \ldots\ldots\ldots (4.3)$$

The measured values of e.m.f. of the above constructed cells and thus determined their ionic transport number, t_{ion} are given in the Table 4.1.

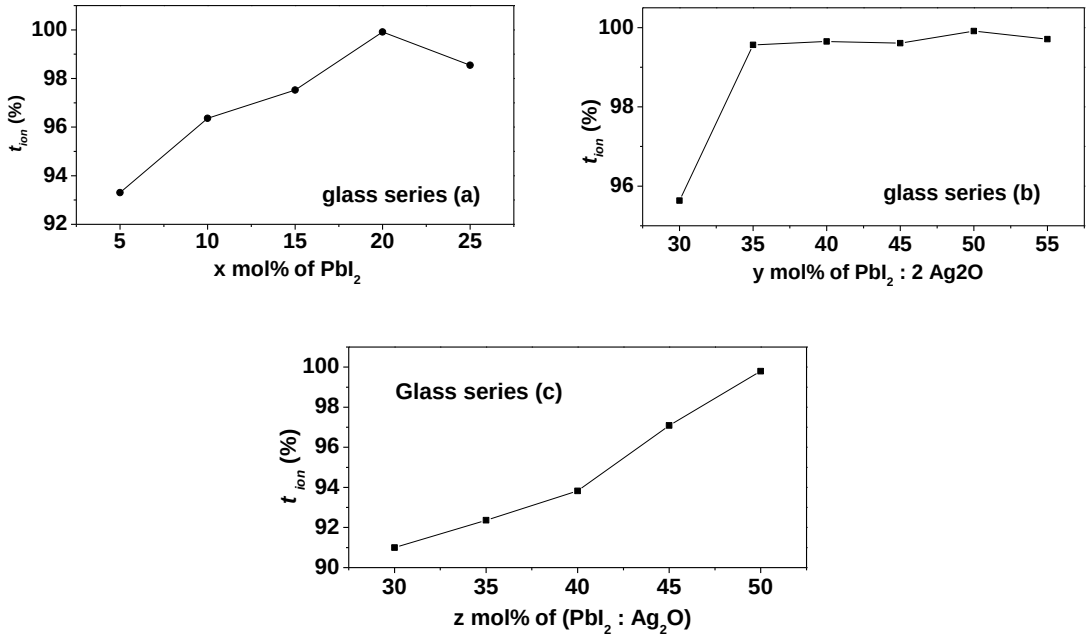

Fig. 4.11. Ion transport number for each glass series as a function of composition.

Table 4.8: Ionic transport number measurements for all three glass series.

Glass series	Sample mole%	cell e.m.f (V)	t_{ion} (%)	Remark
Series (a) $x\ PbI_2$ - (100-x) [Ag_2O - 2(0.7V_2O_5 – 0.3B_2O_3)]	x = 5 %	0.641	93.30	Ionic dominant
	x = 10 %	0.662	96.36	Superionic
	x = 15 %	0.670	97.53	Superionic
	x = 20 %	0.686	99.91	Superionic
	x = 25 %	0.677	98.54	Superionic
Series (b) y (PbI_2:2Ag_2O) - (100-y) [0.7V_2O_5 - 0.3B_2O_3]	y = 30 %	0.657	95.63	Ionic dominant
	y = 35 %	0.684	99.56	Superionic
	y = 40 %	0.685	99.65	Superionic
	y = 45 %	0.684	99.61	Superionic
	y = 50 %	0.686	99.91	Superionic
	y = 55 %	0.685	99.71	Superionic
Series (c) z (PbI_2:Ag_2O) - (90-z) V_2O_5 - 10B_2O_3	z = 30 %	0.626	91.16	Ionic dominant
	z = 35 %	0.632	91.99	Ionic dominant
	z = 40 %	0.645	93.89	Ionic dominant
	z = 45 %	0.667	97.09	Superionic
	z = 50 %	0.686	99.85	Superionic

As shown in the Table 4.1, the ion transport number for all compositions is found to be nearly unity, which suggests that all glass samples are either ionic dominant or superionic in nature. And hence their ion transport properties may be investigated further.

References

1. V. Kundu, R.L. Dhiman, A.S. Maan, D.R. Goyal, Advances in Condensed Matter Physics (2008) Article ID 937054, 1-7.
2. M.A. Frechero, O.V. Quinzani, R.S. Pettigrosso, M. Villar, R.A. Montani, J. Non-Cryst. Solids 353 (2007) 2919.
3. C. F. Drake, J. A. Stephens, B. Yates, J. Non-Cryst Solids 28 (1978) 61.
4. JCPDS-ICDD, Powder Diffraction File No. 740812, 2002.
5. JCPDS-ICDD, Powder Diffraction File No. 701703, 2002.
6. A. K. Varshneya, Fundamentals of Inorganic Glasses, Academic Press, San Diego, 1994.
7. V. Berbenni, A. Marini, S. Scotti, M. Villa, Solid State Ionics 53–56 (1992) 1245–1249.
8. M. Tatsumisago, Y. Shinkuma, T. Saito, T. Minami, Solid State Ionics 50 (1992) 273.
9. Rawson, Material Science Technology 9 (1991) 279.
10. J.E. Garbarczyk, M. Wasiucionek, P. Jozwiak, L. Tykarski, J.L. Nowinski, Solid State Ionics 154– 155 (2002) 367.
11. C. R. Kurjjain, E. A. Sigety, Phys. Chem. Glasses, 9 (1968) 73.
12. C. R. Kurjjain, J. Non-Cryst. Solids 3 (1970) 157.
13. T. K. Bansal, R. G. Mendiratta, Phys. Chem. Glasses 28, 6 (1987) 242.
14. T. Nishida, Y. Takashima, J. Non-Cryst. Solids 94 (1987) 229.
15. T. Satyanaryana et al. , J Al. Com. 482(2009) 283.
16. Y. Dimitriev, V. Dimitrov, M. Arnaudov, J. Mat. Sci. 14 (1979) 723.
17. E. Culea, L. Pop, P. Pascuta, M. Bosca, Journal of Molecular Structure 924–926 (2009) 192.
18. M. Bosca, L. Pop, G. Borodi, P. Pascuta, E. Culea, J. Alloys Compd. 479 (2009) 579.
19. N.F. Uvarov, P. Vanek, M. Savinov, V. Zelezny, V. Studnicka, J. Petzelta, Solid State Ionics 127 (2000) 253.
20. M. Rada, E. Culea, S. Rada, V. Maties, P. Pascuta,J Mater Sci 45 (2010) 1487.
21. K. Funke, Zeit Fur, Phys. Chem., Neue Folge Bd 154 (1987) S–151.
22. C.T. Moynihan, L.P. Boesch, N.L. Laberge, Phy. Chem. Glasses 14 (6) (1973) 122.
23. E.J. Baran, P.J. Aymonino, Anorg. Allg. Chem. 365 (1969) 21.
24. M. Ganguli, K. J. Rao, J. Solid State Chemistry 145 (1999) 65.
25. A. Padmanabham, Y. Gandhi, M.V.N. Padma Rao, M.V.R. Rao, D.V.M. Appaji, IOP Conf. Series: Mat. Sci. Engg. 2 (2009) 012055.
26. C.P.E. Varsamis, E.I. Kamitsos, M. Tatsumisago, T. Minami, J. Non-Cryst. Solids 345-346 (2004) 93.
27. J.R. Frade, V.V. Kharton, A.A. Yaremchenko, E.V. Tsipis, J. Solid State Electrochem. 10 (2006) 96.
28. M. Kawasaki, J. Kawamura, Y. Nakamura, M. Aniya, Solid State Ionics 123 (1999) 259.